Endocochlear potential contributes to hair cell death in TMPRSS3 hearing loss

A. Eliot Shearer[1, 2,**], Yuan-Siao Chen[3#], Stephanie L. Rouse[2#], Xiaohan Wang[2], Janmaris Marin Fermin[2], Kevin TA. Booth[3,4], Jasmine Moawad[5], Nicole Bianca Libiran[5], Jinan Li[3], Hae-Young Kim[1], Michael Hoa[6], Rafal Olszewski[6], Jing-Yu Lei[3], Ernesto Cabrera[3], Douglas J. Totten[3], , Bo Zhao[3], Jeffrey R. Holt[1,2], Rick F. Nelson[3,7,*]

1. Department of Otolaryngology and Communication Enhancement, Boston Children's Hospital. 300 Longwood Avenue, BCH-3129, Boston, MA 02115, USA

2. Department of Otolaryngology Head and Neck Surgery, Harvard Medical School, 25 Shattuck Street, Boston, MA 02115, USA

3. Department of Otolaryngology-Head and Neck Surgery, Indiana University School of Medicine, Indianapolis, IN 46202, USA

4. Department of Medical and Molecular Genetics, Indiana University School of Medicine, Indianapolis, IN 46202, USA

5. Indiana University School of Medicine, Indiana University, Indianapolis, IN 46202, USA

6. Auditory Development and Restoration Program, Neurotology Branch, National Institutes on Deafness and Other Communication Disorders, National Institute of Health (NIH), Bethesda, MD 20892, USA

# Contributed equally

7. Lead contact

Correspondence: *ricnelso@iu.edu and ** eliot.shearer@childrens.harvard.edu

Rick F. Nelson, MD PhD
Walther Hall, C426C
980 West Walnut Street
Indianapolis, IN 46202
(317) 948-9887

Eliot Shearer, MD PhD
BCH 3129
300 Longwood Ave
Boston, MA 02115
617-355-4556

Conflict-of-interest policy: The authors have declared that no conflict of interest exists.

SUMMARY

Pathogenic variants in the gene *TMPRSS3* are a common cause of hearing loss in humans, although the causal mechanisms remain unknown. Previous work has shown that *Tmprss3*$^{Y260X/Y260X}$ mice exhibit normal hair cell development, mechanosensory transduction, and spiral ganglion patterning, but experience rapid hair cell death from P12 to P14 at the onset of hearing. Here, we demonstrate that *Tmprss3*$^{Y260X/Y260X}$ mice display an early and temporary spike in endocochlear potential (EP) prior to the onset of hair cell death. *In vitro* experiments with cochlear explants from *Tmprss3*$^{Y260X/Y260X}$ mice and *in vivo* studies with *Tmprss3*$^{Y260X/Y260X}$ mice crossed with two different mutant models that lacked EP generation promoted hair cell survival. Furthermore, systemic administration of furosemide, a drug that reduces EP *in vivo*, reduced hair cell death in *Tmprss3*$^{Y260X/Y260X}$ mice. These findings suggest that extracellular factors, including EP, play a role in TMPRSS3-related hair cell survival and hearing loss, and suggest that modulating EP could be a therapeutic strategy.

Keywords: TMPRSS3, hair cell degeneration, endocochlear potential, hearing loss, deafness

INTRODUCTION

For the majority of genes associated with hearing loss (HL), the underlying pathologic mechanism is not known. Determining the precise molecular mechanism underlying each form of genetic HL is critical for development of new treatment modalities, currently limited to hearing aids and cochlear implants (CIs), but in the near future may include correction of underlying pathology with molecular or gene therapies. One gene for which the underlying disease mechanism is still elusive is *TMPRSS3*.

Bi-allelic pathogenic variants in *TMPRSS3* cause two forms of sensorineural HL: early-onset severe to profound HL (DFNB10) as well postlingual progressive high frequency HL (DFNB8)(1). *TMPRSS3* is commonly implicated as a cause of human hearing loss(2). We, and others, have previously shown that, unlike other forms of genetic HL, *TMPRSS3*-related HL is associated with variable speech perception outcomes after cochlear implantation in adults, and is correlated with duration of deafness, possibly due to reduced spiral ganglion neuron (SGN) function.(3-5) In contrast, in children with TMPRSS3-related HL, CI outcomes are more positive(6). Given its relatively high contribution to genetic HL and the variable CI outcomes associated *TMPRSS3*-related HL, determination of the function of *TMPRSS3* and how its dysfunction results in HL is critical for a comprehensive understanding of DFNB8/10.

The *TMPRSS3* gene encodes the transmembrane serine protease III protein, a widely expressed protein with multiple tissue-specific isoforms(7). To date, there are over 70 reported pathogenic hearing loss associated variants in *TMPRSS3* (8, 9). In the inner ear, *TMPRSS3* is expressed in inner hair cells (IHCs), outer hair cells (OHCs), and in type II, but not type I SGNs(7, 10, 11). The previously developed *Tmprss3*-null mouse model (*Tmprss3*$^{Y260X/Y260X}$) shows rapid degeneration of cochlear hair cells beginning at the onset of hearing, postnatal day (P) 12 leading to compete loss of hair cells by P14, resulting in profound deafness(7, 11). Hair cells develop normally, but quickly undergo cell death at the onset of hearing, a unique pathology compared to other forms of genetic hearing loss.

The mechanism for hair cell death at the onset of hearing in *Tmprss3*$^{Y260X/Y260X}$ mice is not understood. However, due to the coincident timing of normal development of the endocochlear potential (EP)(12) and rapid hair cell degeneration in *Tmprss3*$^{Y260X/Y260X}$ mice, we hypothesized that EP may play a role in hair cell loss and subsequent deafness in *Tmprss3*$^{Y260X/Y260X}$ mice. The apical surface of cochlear hair cells is bathed in endolymph, which is high in extracellular K^+ and provides the +90 mV EP. Interestingly, the time period at which massive hair cell death occurs in

Tmprss3$^{Y260X/Y260X}$ mice coincides with development of the EP as there is a rapid rise from +16 mV to +60 mV, reaching the mature +90 mV by P15(12). The EP is generated by the cells of the stria vascularis and provides a steep electrochemical gradient that drives sensory transduction current into hair cells, carried primarily by K^+ and Ca^{2+}(13). One route for K^+ efflux from hair cells is via BK channels which are large-conductance, calcium-activated potassium channels. *KCNMA1* is the gene that produces the pore-forming α-subunit of BK channels, which localize on the neck of mature IHCs(11, 14). Normally, *Kcnma1* is first expressed at P12, however, KCNMA1 channels are not detected in IHCs of *Tmprss3*$^{Y260X/Y260X}$ mice(11, 15). Interestingly, KCNMA1-null mice have normal hearing at 4-weeks of age and develop a mild progressive high-frequency hearing loss, based on alterations of OHC function(16). Based upon the temporal correlation between rapid hair cell death with EP maturation, along with alterations in hair cell potassium channel expression, we hypothesize that alterations of EP contributes to hair cell death and hearing loss in *Tmprss3*$^{Y260X/Y260X}$ mice.

Here, we investigated this hypothesis by modifying the intracochlear environment and assessing effects on hair cell survival in *Tmprss3*$^{Y260X/Y260X}$ mice both *in vitro*, using a cochlear explant model, and *in vivo*, crossing *Tmprss3*$^{Y260X/Y260X}$ mice with two mouse strains that lack development of EP. We also measured EP directly in *Tmprss3*$^{Y260X/Y260X}$ mice and show that EP aberration is associated with the rapid hair cell death and hearing loss in these mice. In addition, pharmacologic reduction of the EP with systemic administration of furosemide led to reduction in hair cell death providing a new possible avenue for treatment of this common cause of human hearing loss.

RESULTS

Hair cells show normal early development and function in *Tmprss3*$^{Y260X/Y260X}$ mice.

We evaluated the morphology and function of hair cells in early stages of postnatal development in *Tmprss3*$^{Y260X/Y260X}$ mice prior to the onset of hearing, and before the previously identified rapid and complete hair cell degeneration of inner and outer hair cells of from P12-P14. At P6, the hair cells showed typical stereocilia morphology and cellular arrangement via phalloidin immunostaining (**Figure 1A**). The hair bundle ultrastructure of *Tmprss3*$^{Y260X/Y260X}$ mice is indistinguishable from heterozygous and wildtype littermates. Mechanosensory transduction currents in mouse hair cells are detected at P0 at the base and reach mature levels between P5-P10 in a tonotopic gradient from base to apex(17, 18). We noted typical hair cell uptake of FM1-43, a styryl dye that specifically labels hair cells via uptake through functional sensory transduction channels, at P7 (**Figure 1C**). Consistent with prior reports, we found that *Tmprss3*$^{Y260X/Y260X}$ IHC and OHCs undergo rapid and complete degeneration by P14 (**Figure 1A**). These data indicate normal early development and function of hair cells in *Tmprss3*$^{Y260X/Y260X}$ mice prior to rapid degeneration.

SGN patterning is normal at early stages in *Tmprss3*$^{Y260X/Y260X}$ mice.

Spiral ganglion neurons (SGNs) innervate IHCs and OHCs and consist of Type I and Type II SGNs. Type I SGNs comprise 95% of SGNs, transmit sound information from the IHCs to the central nervous system, and consist of three unique subtypes (IA, IB, IC) based upon single cell transcriptomic profiling(10, 19) and spontaneous firing rates(20). Type II SGNs comprise the remaining 5% of the SGN population, synapse on multiple OHCs and are not essential for sound transmission, but instead are likely involved in damage perception(21). SGNs undergo major refinement in molecular phenotype in the first few postnatal weeks(19). Proper segregation of Type I and Type II SGNs and subtype specification of Type I SGNs is dependent upon the spontaneous activity of hair cells and functional sensory transduction prior to the onset of hearing(19). Genetically engineered mice with defective synaptic transmission or sensory transduction exhibit severe alterations in the Type 1 SGN subtyping(19). TMPRSS3 expression is not detected in Type I SGNs and is limited to only Type II SGNs(10). To test if loss of TMPRSS3 impacted SGN function, we profiled the composition of SGNs in *Tmprss3*$^{Y260X/Y260X}$ mice at early time points (**Figure 2**). The total number of Tuj1-positive SGNs was no different between *Tmprss3*$^{Y260X/Y260X}$ and control mice (**Supplemental figure S1**). Staining with antibodies specific for Type IA (calretinin), Type IB (calbindin), Type IC (BRN3A), and Type II (NGFR) SGNs revealed identical subtype composition between the control mice (*Tmprss3*$^{Y260X/+}$) and *Tmprss3*$^{Y260X/Y260X}$

mice at P11 (**Figure 2A & B**). Despite hair cell degeneration by P14 in *Tmprss3*$^{Y260X/Y260X}$ mice, no significant differences in Type I SGNs were observed at P21.The Type II SGNs were slightly, though significantly, decreased in *Tmprss3*$^{Y260X/Y260X}$ mice at P21. These data demonstrate that loss of expression of TMPRSS3 does not impact activity-dependent subtype patterning of Type 1 SGN and provides further support of that loss of TMPRSS3 does not disrupt hair cell transduction which is critical to IHC development.

Hair cell death in *Tmprss3*$^{Y260X/Y260X}$ mice is mediated by the intracochlear environment.

The endolymph within the scala media is comprised of extracellular fluid containing 157 mM potassium that is dependent upon the KCNJ10 channel of the lateral wall of the cochlea(22). The positive EP within the scala media of 80-100 mV is generated by the stria vascularis and reaches peak levels at P14 at the onset of hearing(23). We had previously shown that inner ear organoids derived from stem cells of *Tmprss3*$^{Y260X/Y260X}$ mice are morphologically and functionally identical to wildtype inner ear organoids and do not undergo the same rapid degeneration seen *in vivo(24)*. Based on prior observations of sudden IHC and OHC death in *Tmprss3*$^{Y260X/Y260X}$ mice between P12-P14(11, 15), we hypothesized that the extracellular environment the EP, in particular, may contribute to the early rapid hair cell death in *Tmprss3*$^{Y260X/Y260X}$ mice. To test this hypothesis and investigate if altering the extracellular environment could prevent hair cell death, we performed cochlear explant cultures. Mouse cochleae were microdissected at P7 and the sensory epithelium was placed in explant culture media for an additional 7 days *in vitro* (DIV). We observed complete preservation of hair cell in the *Tmprss3*$^{Y260X/Y260X}$ mice (**Figure 3**). To determine the length of survival in culture, we cultured P7 *Tmprss3*$^{Y260X/Y260X}$ explants for up to 30 days **(Figure 3)**. While we observed some loss of OHCs with progressively longer culture times, there was no statistically significant difference in hair cell survival between *Tmprss3*$^{Y260X/Y260X}$ explants compared to control *Tmprss3*$^{Y260X/+}$ explants (**Figure 3I**; *n* = 3-5 cultures per condition). This supported our hypothesis that the extracochlear environment causes massive hair cell death in *Tmprss3*$^{Y260X/Y260X}$ mice.

EP measurement in mouse models.

Tmprss3 transcript expression is detected in the rare spindle root cells of the lateral wall and not within the major stria vascularis cells like the marginal, intermediate or basal cells(25). To determine if TMPRSS3 expression alters EP, we first performed EP measurement on adult mice at P28. We observed no difference in mature EP between *Tmprss3*$^{Y260X/Y260X}$ and control mice regardless of sex (**Figure 4A and 4B**).

Next, we sought to evaluate EP dynamics in *Tmprss3*$^{Y260X/Y260X}$ mice during the critical period of EP development from P7 to P24. Similar to our adult measurements above, we directly measured EP in live control and *Tmprss3*$^{Y260X/Y260X}$ mice using glass micropipettes inserted into the scala media. The EP was recorded as the voltage difference between the micropipette's stable positions in the scala media and the scala tympani (**Figure 4A**).

We found that the EP was on average 8.9 mV higher at ages P7-P11 in *Tmprss3*$^{Y260X/Y260X}$ mice compared to *Tmprss3*$^{Y260X/+}$ mice (48.9 ± 16.4 mV vs 40.0 ± 10.0 mV, respectively) (**Figure 4C**). This difference was not statistically different ($p = 0.26$) as measured by a Wilcoxon rank sum test (Mann-Whitney test). The EP was 30 mV higher in *Tmprss3*$^{Y260X/Y260X}$ mice compared to controls when tested at P12-P15 (88.3 ± 8.9 mV vs 58.2 ± 12.9 mV, respectively, $p < 0.0001$) (**Figure 4C**). After the onset of hearing, the EP stabilized at ~90-95 mV at P18-P21, and was not significantly different between *Tmprss3*$^{Y260X/Y260X}$ and control mice (89.2 ± 10.9 mV vs 94.7 ± 5.6 mV). Thus, the premature rise in EP noted here in the *Tmprss3*$^{Y260X/Y260X}$ mice prior to P16 occurred concurrently with previously identified complete hair cell degeneration. The rapid rise in EP from P10 through the onset of hearing at P14 is temporally correlated with the rapid hair cell degeneration between P12-P14 seen in *Tmprss3*$^{Y260X/Y260X}$ mice (**Figure 4D**). This early rise in EP may be a secondary consequence of a yet to be identified role of TMPRSS3 in the lateral wall, the lack of KCNMA1 expression in the *Tmprss3*$^{Y260X/Y260X}$ hair cells, or a consequence of hair cell degeneration.

Reduction of EP *in vivo* prevents hair cell death.

To further investigate the role of the EP on TMPRSS3-mediated hair cell death *in vivo* we crossed the*Tmprss3*$^{Y260X/Y260X}$ line, with the two different mutant mouse lines, *Mitf*$^{+/Mi\text{-wh}}$ *Pou3f4*^{delJ}. Microphthalmia-White (*Mitf*$^{+/Mi\text{-wh}}$) mice are a model for human deafness-pigmentation syndromes, Waardenburg syndrome type 2a and Tietz syndrome, caused by mutations in *MITF* gene and characterized by profound deafness along with melanocyte deficiency. *Mitf*$^{+/Mi\text{-wh}}$ mice carry heterozygous mutations in the Mitf gene and exhibit profound hearing loss, and an EP that is less than 20 mV in adult mice(26, 27). Progressive OHC loss is observed in the *Mitf*$^{+/Mi\text{-wh}}$ mice by P28 in a tonotopic gradient from base to apex(26). *Pou3f4*^{delJ} mice are a model for human X-linked nonsyndromic deafness (DFN3) caused by mutations in the gene *POU3F4*, a transcription factor. Compared to controls, *Pou3f4*^{delJ} mice have reduced EP (85 mV vs. 38 mV, respectively)(28). POU3F4 is required for generation of the EP, but not for generation of cochlear hair cells(28).

As anticipated, we confirmed a lack of EP in the *Tmprss3*$^{Y260X/+}$*;Mitf*$^{+/Mi\text{-wh}}$ mice at one month of age ($n = 3$, EP = 0 mV). Unsurprisingly, due to complete lack of EP, these mice had profound

hearing loss as measured by ABR at all frequencies tested at P16 (**Supplemental Figure S2**). Next, we examined the loss of EP on hair cell survival and, intriguingly, there was a dramatic preservation of both IHCs and OHCs inner and outer hair cells in the *Tmprss3*$^{Y260X/Y260X}$*;Mitf*$^{+/Mi\text{-}wh}$ double mutant mice (**Figure 5A&B**). While there was robust preservation of IHCs in *Tmprss3*$^{Y260X/Y260X}$*;Mitf*$^{+/Mi\text{-}wh}$ mice (**Figure 5B**), we observed a base to apex gradient of OHC loss in *Tmprss3*$^{Y260X/Y260X}$*;Mitf*$^{+/Mi\text{-}wh}$ mice which was not significantly different than *Tmprss3*$^{Y260X/+}$*;Mitf*$^{+/Mi\text{-}wh}$ mice, and is consistent with previously reported hair cell loss in the mouse line *Mitf*$^{+/Mi\text{-}wh}$ (**Figure 5B**)(29). We also observed no significant progression in OHC cell death P16 to P21 (**Figure 5B**).

To confirm this finding in an additional model that does not exhibit progressive hair cell loss, we generated *Tmprss3*$^{Y260X/Y260X}$*;Pou3f4*$^{delJ/Y}$ (male) or *Tmprss3*$^{Y260X/Y260X}$*;Pou3f4*$^{delJ/delJ}$ (female) double mutant mice. Analysis of P48 mice revealed complete preservation of both IHCs and OHCs regardless of sex (**Figure 5C&D**). Despite complete hair cell preservation, ABR testing of adult (P28) double mutant mice (*Tmprss3*$^{Y260X/Y260X}$*;Pou3f4*^{delJ}) demonstrated profound hearing loss like we observe in *Tmprss3*$^{Y260X/Y260X}$ and in *Pou3f4*^{delJ} mutant mice (**Supplemental Figure S3**). This hearing result is expected given the suspected low EP in double mutant mice (*Tmprss3*$^{Y260X/Y260X}$*;Pou3f4*^{delJ}). Taken together, these data confirm that EP *in vivo* plays a major role in the pathogenesis of hair cell death in *Tmprss3*$^{Y260X/Y260X}$ mice.

KCNMA1 channels are not expressed in surviving hair cells

Prior proteomic analysis of cochlea from control and *Tmprss3*$^{Y260X/Y260X}$ mice revealed reduced expression of APOA1, a KCNMA1 associated protein(11).Immunohistochemical staining demonstrated complete absence of KCNMA1 puncta near the apex of *Tmprss3*$^{Y260X/Y260X}$ hair cells at P12 prior to degeneration(11). To determine if hair cell survival after P14 restored expression of KCMA1, we performed antibody labelling in *Tmprss3*$^{Y260X/Y260X}$*;Mitf*$^{+/Mi\text{-}wh}$ mice. Control mice (*Tmprss3*$^{Y260X/+}$*;Mitf*$^{+/+}$) showed KCNMA1 expression increased from P12-P15 in the previously reported base-apex gradient(14) during this time period (**Figure 6A&B**). Conversely, while IHCs and OHCs survive due to the reduced EP in the *Tmprss3*$^{Y260X/+}$*;Mitf*$^{+/Mi\text{-}wh}$ model (described above), there is complete lack of expression of KCNMA1 in the *Tmprss3*$^{Y260X/Y260X}$*;Mitf*$^{+/Mi\text{-}wh}$ mice at P15 (**Figure 6A&B**). Therefore, although reduction in EP results in hair cell survival in *Tmprss3*$^{Y260X/Y260X}$ mice, expression of KCNMA1 requires expression of functional TMPRSS3.

Pharmacologic reduction in EP rescues hair cells in *Tmprss3*$^{Y260X/Y260X}$ mice

Based on our results showing preservation of *Tmprss3*$^{Y260X/Y260X}$ hair cells with *in* vivo reduction of EP in two separate two-strain mouse models, we hypothesized that pharmacologic reduction of EP would also preserve hair cells in *Tmprss3*$^{Y260X/Y260X}$ mice. Furosemide acts on the Na^+-K^+-$2Cl^-$ co-transporter in the kidney to induce diuresis[29]. Additionally, action of furosemide on the co-transporter in the cochlea leads to transient reduction in the EP(30). We tried varying amounts of furosemide injected intraperitoneally (50-200 mg/kg) between P10 and P14 and found that 200 mg/kg injected once daily was tolerated when saline was administered twice daily to counter expected diuresis. In a litter of 9 *Tmprss3*$^{Y260X/Y260X}$ mice, two served as controls with daily administration of saline only, and seven were injected with 200 mg/kg furosemide daily from P10-P14. Animals treated with the furosemide showed significantly increased inner and outer (in Apex only) hair cell survival compared to saline treated controls (IHC: $p = 0.0003$ for Apex, $p = 0.0008$ for Mid, $p=0.006$ for Base; OHC: $p=0.009$ for Apex, Nonparametric ANOVA with Tukey's post hoc test, **Figure 7**). In contrast, administration of 100 mg/kg daily furosemide led to minimal or no hair cell preservation ($n = 6$, data not shown). These results suggest that pharmacologic reduction in EP leads to preservation of cochlear hair cells that lack functional TMPRSS3.

DISCUSSION

The endocochlear potential (EP) is integral to cochlear physiology, with its functional significance becoming especially apparent during and after the onset of auditory function. In mature mice, EP typically stabilizes within the range of +80 to +100 mV. This stabilization is critical for sustaining the large electrochemical gradient necessary for the transduction process within hair cells. Genetic defects that impact the formation or maintenance of EP are associated with hearing impairment in both mice and humans. In this context, our findings introduce EP abnormalities as a contributing factor to the pathologic mechanism of DFNB8/10 hearing loss.

Our prior observation that inner ear organoids derived from *Tmprss3*$^{Y260X/Y260X}$ mice did not show hair cell degeneration indicated a possible extracellular mechanism for degeneration(24). This observation led us to explore the consequence of direct culturing of cochlear explants from control and *Tmprss3*$^{Y260X/Y260X}$ mice. We found that in culture, we could prevent the rapid hair cell degeneration that occurs between P12-P14 in *Tmprss3*$^{Y260X/Y260X}$ mice (**Figure 3**), further supporting our hypothesis that EP was an underlying contributor to the hair cell (HC) death.

To understand the directional effect of loss of Tmprss3 on EP and the magnitude, we measured EP from the cochleae of *Tmprss3*$^{Y260X/Y260X}$ and control mice. Surprisingly, we observed abnormally high EP levels in the maturing cochlea of *Tmprss3*$^{Y260X/Y260X}$ mice compared to controls (**Figure 4**). To date, many reported defects in EP that result in deafness are due to a reduction or failure to generate EP(31-33). While the EP measured in the maturing cochlea of *Tmprss3*$^{Y260X/Y260X}$ mice was significantly elevated, it was not outside the physiologically normal range for mature cochlea (>P14). These findings indicate that maturing hair cells may lack the resilience required to withstand premature elevations in EP, and part of the hair cell maturation process entails equipping the hair cells to survive in environments characterized by high ionic gradients.

Next, we asked if reducing EP *in vivo* through genetic manipulation could preserve hair cells in the *Tmprss3*$^{Y260X/Y260X}$ mice. EP is maintained by the stria vascularis, which is a specialized epithelial layer located on the lateral wall of the cochlear duct. This structure plays a critical role in regulating the ionic composition of the endolymph, the fluid that fills the scala media and bathes the hair cells of the inner ear. The transcription factors *Pou3f4* and *Mitf* share critical roles in influencing the function of the stria vascularis, particularly through their effects on cellular development and integrity, which are essential for EP formation and maintenance. Mutant mouse models for both genes result in significant reduction of EP(26, 28). We crossed *Tmprss3*$^{Y260X/Y260X}$ mice with both the *Mitf*$^{+/Mi\text{-}wh}$ mutant and the *Pou3f4*^{delJ} mutant. By eliminating the supraphysiologic

rise in EP, we saw significant HC survival at the critical P12-P14 time point and HC survival rates mimicked litter mate controls (**Figure 5**).

Complicating efforts to tease apart the mechanism(s) driving TMPRSS3-related hearing loss is the lack of specific, well-validated antibody to detect TMPRSS3 protein in mouse cochleae. However, *Tmprss3* RNA in mouse cochleae is express throughout the cells of organ of Corti including inner and outer hair cells and the spindle root cells, but no expression was detected within the stria vascularis and was not detected in type II spiral ganglion neurons(7, 9). These data suggests that TMPRSS3 functions within the sensory hair cells of the cochlea. To date there are limited number of potential downstream targets for TMPRSS3. Previously, the outward rectifying potassium channel, KCNMA1, was shown to be absent in the hair cells of P12-P13 *Tmprss3*$^{Y260X/Y260X}$ mutants and has been hypothesized to be a downstream target of TMPRSS3. To test if KCNMA1 was restored in surviving *Tmprss3*$^{Y260X/Y260X}$ hair cells *in vivo*, we analyzed the KCNMA expression in double mutant mice. Compared to controls (*Tmprss3*$^{Y260X/+}$ *; Mitf*$^{+/+}$), surviving hair cells in the *Tmprss3*$^{Y260X/Y260X}$*;Mitf*$^{+/Mi\text{-}wh}$ model also did not show expression KCNMA1 from P12 to P15, (**Figure 6**), indicating that KCNMA1 expression in surviving hair cells requires TMPRSS3. It should also be noted that KCNMA1 mutant mice are not profoundly deaf and develop a late onset high frequency mildly progressive hearing loss(16). The role KCNMA1 loss plays in the pathobiology of TMPRSS3-related hearing loss, remains unclear.

Both *Pou3f4*^{delJ} mice and *Mitf*$^{+/Mi\text{-}wh}$ mice are deaf due to a failure to generate EP and both lines have progressive HC loss. While the decrease in EP resulted in significant HC survival for TMPRSS3 mutants crossed with either line, ultimately these crosses are still deaf. To circumvent the effects of genetic manipulation, we sought to regulate EP pharmacologically, by manipulating electrolyte balance. Using furosemide, a loop diuretic, we treated *Tmprss3*$^{Y260X/Y260X}$ mice with varying dosing regiments. When *Tmprss3*$^{Y260X/Y260X}$ mice were treated systemically with this drug, we saw an increase in HC survival (**Figure 7**), during the critical P12-P14 time point, primarily in the apex. HC survival was not as robust to what was seen with complete oblation of EP via genetic manipulation (**Figures 5**). It is unclear to what extent and duration furosemide lowered EP in treated animals and further studies are needed to explore dosing and its impact on regulating EP. Nevertheless, loop diuretics may provide a mechanism to extend the therapeutic window for *TMPRSS3* hearing loss in humans. This is particularly important given that humans develop hearing, and EP, *in utero* and may be born with permanent hair cell loss. Pharmacologic reduction of EP may provide a method for preservation of cochlear hair cells to allow for later gene therapy intervention(29).

In humans, pathogenic variants in *TMPRSS3* result in two distinct phenotypes: congenital severe-to-profound hearing loss (DFNB10) and post-lingual progressive hearing loss (DFNB8). We suspect the DFNB10 phenotype to be associated with a toxic rise in EP resulting in HC death and profound hearing loss. Whereas the pathomechanism for DFNB8, remains elusive, but is less likely tied to EP, given its milder phenotype. More work is needed to understand the full extent of TMPRSS3's role in auditory function.

In summary, we implicate defects in EP as the possible pathomechanism underlying severe-profound *TMPRSS3*-related hearing loss. We show through multiple lines of evidence that hearing loss in *Tmprss3*$^{Y260X/Y260X}$ mice is due to a toxic premature rise of EP which results in subsequent HC death just prior to and at the onset of hearing. We also show by manipulating EP, either by genetic manipulation or pharmacologically, HC death can be eliminated or diminished, indicating a mechanism for treatment of *TMPRSS3*-related hearing loss.

METHODS

Resource availability

Lead contact

Further information and requests for resources and reagents should be directed to and will be fulfilled by the lead contact, Rick Nelson (ricnelso@iu.edu)

Materials availability

Research reagents generated in this study will be distributed upon request to other investigators under MTA.

Data and code availability

- Microscopy data reported in this paper will be shared by the lead contact upon request.
- This paper does not report original code.
- Any additional information required to reanalyze the data reported in this work paper is available from the lead contact upon request.

Experimental model details

All animal experiments were performed in compliance with the guidelines provided by the Institutional Animal Care and Use Committee (IACUC) at Indiana University School of Medicine (protocol #23148) or at Boston Children's Hospital (protocol # 000013339). The mice were housed in a temperature-controlled room with 12-hr light/dark cycle and had free access to water and food. Both male and female were used in all experiments (P7-P48). *Tmprss3*$^{Y260X/Y260X}$ mice (C3HeB/FeJ background) were provided from Dr. Michel Guipponiat University of Geneva. C3HeB/FeJ (RRID:IMSR_JAX:000658), C3HeB/FeJ-*Pou3f4*$^{del-J}$/J (RRID:IMSR_JAX:004406), and B6.Cg-*Mitf*$^{Mi-wh}$/J (RRID:IMSR_JAX:000057) mice were purchased from Jackson laboratory. *Tmprss3*$^{Y260X/Y260X}$;*Pou3f4*$^{del-J}$ double mutation mice were generated by crossbreeding *Tmprss3*$^{Y260X/Y260X}$ and C3HeB/FeJ-*Pou3f4*$^{del-J}$/J. *Tmprss3*$^{Y260X/Y260X}$;*Mitf*$^{Mi-wh}$/J hybrid strain were generated from backcrossing B6.Cg-*Mitf*$^{Mi-wh}$/J to C3HeB/FeJ to obtain C3.Cg-*Mitf*$^{Mi-wh}$ followed by crossbreeding *Tmprss3*$^{Y260X/Y260X}$ and C3.Cg-*Mitf*$^{Mi-wh}$. The *Mitf*$^{+/Mi-wh}$ mouse recapitulates human Waardenburg syndrome in that the mutation functions in a dominant-negative fashion. Heterozygous *Mitf*$^{+/Mi-wh}$ mice have profound hearing loss, lack of EP, and altered fur coloring. *Mitf*$^{Mi-wh/Mi-wh}$ share these same characteristics but are less viable and poor breeders. For this reason we used *Tmprss3*$^{Y260X/Y260X}$;*Mitf*$^{+/Mi-wh}$ as our experimental animals.

METHOD DETAILS

Genotyping

Genomic DNA was prepared from the mouse ear notch with QuickExtract™ DNA extraction solution following manufactory instruction. For the *Tmprss3*$^{Y260X/Y260X}$ mice PCR amplicons were generated using 10 pmol of each primer (TMP3SEQ_F and TMP3SEQ_R) and then sequenced with TMP3SEQ_F primer to determine the genotype of the mice. For *Pou3f4*$^{del\text{-}J}$ mice the Taqman qPCR protocol (Protocol 41591 from Jackson Laboratory) was performed on QuantStudio 5 and the 2^(-ΔCt) values of *Pou3f4* and housekeeping *Apob* gene was calculated. The known wild-type, hemizygous, and homozygous were performed as the control to determine the genotype of unknown sample. For *Mitf*$^{+/Mi\text{-}wh}$ mice direct sequencing was performed using a commercial lab (TransNetyx). The list of all primers and sequences used for genotyping can be found in the Key resources table.

Sex as a biological variable

Our study examined male and female animals, and similar findings are reported for both sexes.

SEM

The P14 mice were euthanized with decapitation. The cochlea was removed from the temporal bone and fixed for 24 h with 2.5% glutaraldehyde in 0.1 M sodium cacodylate buffer (pH 7.4) containing 2 mM $CaCl_2$, washed in buffer. The sensory epithelium was harvested by removing the bony cartilage, the lateral wall, Reissner's membrane, tectorial membrane, and the cochlear nervous tissue under the stereomicroscope followed by post-fixed for 1 h with 1% OsO_4 in 0.1 M sodium cacodylate buffer and washed. The tissues were dehydrated via an ethanol series, critical point dried from CO_2 and sputter-coated with gold. The morphology of the HCs was examined in a FEI Quanta 200 scanning electron microscope (ThermoFisher, Hillsboro, OR) and photographed.

FM1-43FX Staining

The P7 pups were euthanized with decapitation. The cochlea was removed from the temporal bone and placed in the ice-cold DMEM/F12 medium. The sensory epithelium was harvested by removing the bony cartilage, the lateral wall, Reissner's membrane, tectorial membrane, and the cochlear nervous tissue under the stereomicroscope prior to FM™ 1-43FX staining. The 10 mM stock solution of FM™ 1-43FX was prepared in DMEM/F12. The sensory epithelium was stained with 10 mM FM™ 1-43FX for 30 secs at room temperature (RT) and immediately washed with

DMEM/F12. The tissue was transferred to the glass slide within DMEM/F12, covered with coverslips, visualized on Leica DMi8 microscopy equipped with epifluorescence optics and Leica Y3 filter cube (excitation 545 nm, emission 605 nm).

SGN subtypes

The P11 and P21 pups were euthanized with decapitation. The cochlea was removed from the temporal bone and fixed with 4% paraformaldehyde overnight at 4°C. Cochlea were then decalcified in 120 mM ethylenediaminetetraacetic acid (EDTA) for 1 days (P11) or 3 days (P21) at RT. The EDTA were refreshed daily, and the elasticity of bone structure was checked to confirm the complete decalcification. The cochlea was cryoprotected in 30% sucrose in PBS and embedded in TFM™ Tissue Freezing Medium. Mid-modiolarections of 6 μm were cut on a cryostat and air-dried for 2 hr. The sections were permeabilized with 0.5% Triton X-100 in PBS for 10 mins at RT, blocked with 5% goat serum in PBS overnight at 4°C, and incubated with primary antibody (Tubulin Beta 3 for type I, Calretinin for type IA, Calbindin for type IB, Brn-3a for type IC, NGFR for type II spiral ganglion neurons) in 5% goat serum in PBS overnight at 4°C. After washing with 0.01% Trixon X-100 in PBS three times for 10 mins each, the sections were incubated with secondary antibodies (Alexa Fluor 488 conjugated goat anti-rabbit IgG, Alexa Fluor 647 conjugated goat anti-mouse IgG1, Alexa Fluor 568 conjugated goat anti-mouse IgG2a, Alexa Fluor 647 conjugated goat anti-rabbit IgG) in 5% goat serum in PBS for 1 hr at RT. The sections were washed and mounted with ProLong™ Gold Antifade Mountant with DAPI. Staining was visualized on Leica DMi8 microscopy equipped with epifluorescence optics. The percentage of SGN subtypes were quantified by calculating the number of immunopositive cells for each marker relative to the total number of SGNs (Figure 2). The total number of type I SGNs was determined by counting TUJ1-positive cells within a 10,000 μm³ volume, defined as a 100 μm × 100 μm area with a depth of 1 μm (Figure S1). Details of all antibodies used, including the source and catalogue number, are included in the Key Resources table.

Mouse Cochlea Explant Culture

The explant cultures were performed on both P14 and P35 equivalent explants. For P14 equivalent explants, pups from *Tmprss3*$^{Y260X/Y260X}$ and *Tmprss3*$^{+/-}$ control littermates were euthanized with decapitation at P7. The sensory epithelium was harvested by removing the bony cartilage, the lateral wall, Reissner's membrane, tectorial membrane, and the cochlear nervous tissue under the stereomicroscope. The sensory epithelium was transfer to 6-well Millicell® Cell Culture Inserts with Pasteur pipette and cultured for 7 days at 37°C in DMEM/F12 medium supplemented with 100 mg/ml Normocin. For P35 equivalent cochlear explants, cochleae were

harvested from *Tmprss3*$^{Y260X/Y260X}$ animals and *Tmprss3*$^{+/-}$ control littermates at P5, plated on glass cover slip, and cultured in 1% FBS, HEPES, MEM + GlutaMax for up to 30 days (D30, equivalent of P35). The sensory epithelium was then fixed with 4% PFA for 20 mins at RT and stained for Myosin7a. Details of all antibodies used, including the source and catalogue number, are included in the Key Resources table.

Physiologic auditory system evaluation in mice

Auditory evaluation using auditory brainstem response (ABR) and otoacoustic emissions (OAEs) were performed as described previously(34).

EP measurement

For P7-P24 mice, measurement of EP was performed while mice were fully anesthetized using ketamine/xylazine and immobilized in the ventral position. The head was further immobilized and stabilized using a suture passed around the maxillary central incisors. Sterile technique was used throughout the procedure. We first began with a midline incision to expose the trachea. After dividing the strap muscles, a simple tracheotomy was performed to allow CO2 egress during immobilization which can lead to reduction in EP[12]. The left bulla was then identified and dissected allowing exposure of the cochlea. A 1 mm diamond bit on a highspeed drill was used to remove the bone just above the basal turn lateral to the round window membrane. Care was taken to not disrupt the membranous labyrinth. A pulled-glass capillary microelectrode (3-5 MΩ) was filled with 150 mM KCl and mounted on a micromanipulator. The ground electrode was placed into neck soft tissue. The microelectrode was then advanced into the scala media through the stria vascularis while measuring the response. Voltage was recorded before advancing into the scala media and set as 0mV reference. The DC voltage was amplified (AxoPatch 200B Patch Clamp Amplifier, Molecular Devices) x 10 and continuously acquired using pCLAMP (Axoscope 11). An appropriate potential was identified when a measurement was stable for at least 5 seconds and the potential disappeared with advancement of the microelectrode into the scala vestibuli.

For P28 mice, measurement of EP was performed as previously described[12]. Briefly, P28 mice were anesthetized with 2,2,2-tribromoethanol (T4842, Sigma-Aldrich, St. Louis, MO, USA) at a dose of 0.35 mg/g body weight. EP measurements were made using glass microelectrodes inserted into the round window and through the basilar membrane of the first turn of the cochlea. Data were recorded digitally (Digidata 1440A and AxoScope 10; Axon Instruments) and analyzed using Clampfit10 (RRID: SCR_011323, Molecular Devices, San Jose, CA, USA). Six *Tmprss3*$^{Y260X/Y260X}$ and six control mice with equal ratios of male and female mice were evaluated.

All members of the research team were blinded to the genotype of the mice during EP testing. The two groups of mice were handled similarly to control for confounding variables (e.g. cage location, feeding time).

Whole Mount Immunofluorescence

The pups between P16 and P31 were euthanized with decapitation. Cochlea were then removed from the temporal bone. Cochlea were then decalcified in 120 mM EDTA for three to four days at room temp. EDTA was refreshed daily with sponginess checked to confirm complete decalcification. The sensory epithelium was harvested by removing the bony cartilage, the lateral wall, Reissner's membrane, tectorial membrane, and the cochlear nervous tissue under the stereomicroscope prior to permeabilization by 1xPBS/0.5% TritonX-100 at room temperature. Tissue was blocked overnight in 5% goat serum/1x PBS in 4°C and incubated with primary antibody (Myo7a for hair cells) in 5% goat serum in PBS overnight at 4°C. After washing with 0.01% Trixon X-100 in PBS three times for 10 mins each, the sections were incubated with secondary antibodies (Alexa Fluor 568 conjugated goat anti-rabbit IgG, Alexa Fluor 555 conjugated goat anti-rabbit IgG, Alexa Fluor 488 conjugated goat anti-mouse IgG2a) in 5% goat serum in PBS for 1 hr at RT. Tissue was washed again 3 times in 1x PBS/0.01% TritonX-100 for 10 min at room temperature. Hoechst 33342 in 1X PBS was added after the last wash. Tissue was briefly rinsed with 1x PBS and transferred onto a slide. Utilizing the stereoscope orient the tissue so hair cells are facing up. Wick away any remaining PBS and add a drop of Invitrogen™ ProLong™ Gold Antifade Mountant with DNA Stain DAPI. Make sure the hair cells are still oriented facing up then gently place the coverslip onto the tissue and let it dry overnight at room temp. Slide was visualized using Leica DMi8 microscopy, Zeiss LSM700, and LSM880. Hair cell count analysis was performed manually using Image J. Details of all antibodies used, including the source and catalogue number, are included in the Key Resources table.

KCNMA1 Quantification

For KCNMA1 quantification, blocking was performed for 1 hour in 2.5% normal donkey serum and stained at 4°C overnight with primary antibodies (mouse anti-Myo7a, mouse anti-Parvalbumin, and rabbit KCNMA1/KCa 1.1). After washing with PBS, samples were incubated with secondary antibody (Alexa Fluor 488 conjugated goat anti-mouse IgG2a, Alexa Fluor 555 conjugated goat anti-rabbit IgG) and Alexa Fluor™ Plus 405 Phalloidin. Confocal imaging was performed using 10X air and 63X oil-immersion objectives with Carl Zeiss LSM 800 confocal microscope. Maximum intensity projection images were generated in Image J. KCNMA1 punctae were counted using automated quantification with Image J.

Pharmacologic reduction of EP using furosemide

Mice were injected intraperitoneally with varying amounts of furosemide diluted in saline from P10-P14 from 50 mg/kg to 200 mg/kg. A dose of 200 mg/kg daily with twice daily saline boluses (100 uL/g) had previously been shown to be well tolerated and effectively reduce the EP in mice(35).

Quantification and Statistical Analysis

Data are presented as mean ± SD and were derived from at least 3 independent experiments unless otherwise indicated. Statistical analysis was carried out in Graphpad Prism 9, SAS version 9.4 (SAS Institute, Cary, NC), and R software (R Foundation for Statistical Computing, http://www.r-project.org/). The exact Wilcoxon rank sum test (exact Mann-Whitney test) was used to compare groups for data that were not normally distributed and unpaired T-test was used to compare group means for normally distributed data. The nonparametric ANOVA with Tukey's post hoc test(36, 37) was used to compare untreated and treated mice in base, middle and apex cochlear turns. All statistical tests were two-sided, with statistical significance set at $\alpha = 0.01$.

Study Approval

All animal experiments were approved and performed in compliance with the guidelines provided by the Institutional Animal Care and Use Committee (IACUC) at Indiana University School of Medicine (protocol #23148) or at Boston Children's Hospital (protocol # 000013339).

Data Availability

Values underlying graphed data and reported means presented in both the main text and supplemental material are included in the Supporting Data Values file.

AUTHOR CONTRIBUTIONS

Conceptualization, E.S., J. H., R.F.N.; methodology, E.S., Y.C., S.R., J.F., J.M., N.L., E.C., D.T., M.H., R.O., X.W., J.L., HY.K., JY.L., K.T.B., B.Z., J.H., R.N.; investigation, E.S., Y.C., S.R., J.F., J.M., N.L., E.C., D.T., M.H., R.O., X.W., J.L., HY.K., JY.L., K.T.B., B.Z., J.H., R.N.; resources, E.S., J. H., R. N.; writing – original draft, E.S., R. N.; writing -review & editing, E.S., M.H., K.T.B., J.H., R. N.; visualization, E.S., J. H., R. N.; supervision, E.S., J. H., R. N.; funding acquisition, E.S., D.T., M.H., J.H., B.Z., R. N.;

ACKNOWLEDGEMENTS

This work was supported by a pilot grant from the Awards Committee of the Research Executive Council at Boston Children's Hospital (A.E.S.); NIH K08DC019716 (A.E.S), R01DC018785 (B.Z.), K08DC016034 and R01DC020574 (R.N.), ZIA DC000088 (M.H.), Biomedical research Grant from Indiana University (R.N.), American Academy of Otolaryngology CORE grant (D.T.). Funding was also provided by the Hernandez Family Fund (J.H. and A.E.S.).

DECLARATION OF INTEREST

The authors declare that they have no competing interests.

REFERENCES

1. Weegerink NJ, Schraders M, Oostrik J, Huygen PL, Strom TM, Granneman S, et al. Genotype-phenotype correlation in DFNB8/10 families with TMPRSS3 mutations. *J Assoc Res Otolaryngol.* 2011;12(6):753-66.
2. Nisenbaum E, Yan D, Shearer AE, de Joya E, Thielhelm T, Russell N, et al. Genotype-Phenotype Correlations in TMPRSS3 (DFNB10/DFNB8) with Emphasis on Natural History. *Audiol Neurootol.* 2023;28(6):407-19.
3. Eppsteiner RW, Shearer AE, Hildebrand MS, Deluca AP, Ji H, Dunn CC, et al. Prediction of cochlear implant performance by genetic mutation: the spiral ganglion hypothesis. *Hear Res.* 2012;292(1-2):51-8.
4. Shearer AE, Eppsteiner RW, Frees K, Tejani V, Sloan-Heggen CM, Brown C, et al. Genetic variants in the peripheral auditory system significantly affect adult cochlear implant performance. *Hear Res.* 2017;348:138-42.
5. Tropitzsch A, Schade-Mann T, Gamerdinger P, Dofek S, Schulte B, Schulze M, et al. Variability in Cochlear Implantation Outcomes in a Large German Cohort With a Genetic Etiology of Hearing Loss. *Ear Hear.* 2023;44(6):1464-84.
6. Holder JT, Morrel W, Rivas A, Labadie RF, and Gifford RH. Cochlear Implantation and Electric Acoustic Stimulation in Children With TMPRSS3 Genetic Mutation. *Otol Neurotol.* 2021;42(3):396-401.
7. Liu W, Lowenheim H, Santi PA, Glueckert R, Schrott-Fischer A, and Rask-Andersen H. Expression of trans-membrane serine protease 3 (TMPRSS3) in the human organ of Corti. *Cell Tissue Res.* 2018;372(3):445-56.
8. Azaiez H, Booth KT, Ephraim SS, Crone B, Black-Ziegelbein EA, Marini RJ, et al. Genomic Landscape and Mutational Signatures of Deafness-Associated Genes. *Am J Hum Genet.* 2018;103(4):484-97.
9. Chen YS, Cabrera E, Tucker BJ, Shin TJ, Moawad JV, Totten DJ, et al. TMPRSS3 expression is limited in spiral ganglion neurons: implication for successful cochlear implantation. *J Med Genet.* 2022;59(12):1219-26.
10. Shrestha BR, Chia C, Wu L, Kujawa SG, Liberman MC, and Goodrich LV. Sensory Neuron Diversity in the Inner Ear Is Shaped by Activity. *Cell.* 2018;174(5):1229-46 e17.
11. Molina L, Fasquelle L, Nouvian R, Salvetat N, Scott HS, Guipponi M, et al. Tmprss3 loss of function impairs cochlear inner hair cell Kcnma1 channel membrane expression. *Hum Mol Genet.* 2013;22(7):1289-99.
12. Li Y, Liu H, Zhao X, and He DZ. Endolymphatic Potential Measured From Developing and Adult Mouse Inner Ear. *Front Cell Neurosci.* 2020;14:584928.
13. Morell RJ, Olszewski R, Tona R, Leitess S, Wafa TT, Taukulis I, et al. Noncoding Microdeletion in Mouse Hgf Disrupts Neural Crest Migration into the Stria Vascularis, Reduces the Endocochlear Potential, and Suggests the Neuropathology for Human Nonsyndromic Deafness DFNB39. *J Neurosci.* 2020;40(15):2976-92.
14. Pyott SJ, Glowatzki E, Trimmer JS, and Aldrich RW. Extrasynaptic localization of inactivating calcium-activated potassium channels in mouse inner hair cells. *J Neurosci.* 2004;24(43):9469-74.
15. Fasquelle L, Scott HS, Lenoir M, Wang J, Rebillard G, Gaboyard S, et al. Tmprss3, a transmembrane serine protease deficient in human DFNB8/10 deafness, is critical for cochlear hair cell survival at the onset of hearing. *J Biol Chem.* 2011;286(19):17383-97.
16. Ruttiger L, Sausbier M, Zimmermann U, Winter H, Braig C, Engel J, et al. Deletion of the Ca2+-activated potassium (BK) alpha-subunit but not the BKbeta1-subunit leads to progressive hearing loss. *Proc Natl Acad Sci U S A.* 2004;101(35):12922-7.

17. Kim KX, and Fettiplace R. Developmental changes in the cochlear hair cell mechanotransducer channel and their regulation by transmembrane channel-like proteins. *J Gen Physiol.* 2013;141(1):141-8.
18. Lelli A, Asai Y, Forge A, Holt JR, and Geleoc GS. Tonotopic gradient in the developmental acquisition of sensory transduction in outer hair cells of the mouse cochlea. *J Neurophysiol.* 2009;101(6):2961-73.
19. Sun S, Babola T, Pregernig G, So KS, Nguyen M, Su SM, et al. Hair Cell Mechanotransduction Regulates Spontaneous Activity and Spiral Ganglion Subtype Specification in the Auditory System. *Cell.* 2018;174(5):1247-63 e15.
20. Liberman MC. Auditory-nerve response from cats raised in a low-noise chamber. *J Acoust Soc Am.* 1978;63(2):442-55.
21. Liu C, Glowatzki E, and Fuchs PA. Unmyelinated type II afferent neurons report cochlear damage. *Proc Natl Acad Sci U S A.* 2015;112(47):14723-7.
22. Marcus DC, Wu T, Wangemann P, and Kofuji P. KCNJ10 (Kir4.1) potassium channel knockout abolishes endocochlear potential. *Am J Physiol Cell Physiol.* 2002;282(2):C403-7.
23. Sadanaga M, and Morimitsu T. Development of endocochlear potential and its negative component in mouse cochlea. *Hear Res.* 1995;89(1-2):155-61.
24. Tang PC, Alex AL, Nie J, Lee J, Roth AA, Booth KT, et al. Defective Tmprss3-Associated Hair Cell Degeneration in Inner Ear Organoids. *Stem Cell Reports.* 2019;13(1):147-62.
25. Gu S, Olszewski R, Taukulis I, Wei Z, Martin D, Morell RJ, et al. Characterization of rare spindle and root cell transcriptional profiles in the stria vascularis of the adult mouse cochlea. *Sci Rep.* 2020;10(1):18100.
26. Ni C, Zhang D, Beyer LA, Halsey KE, Fukui H, Raphael Y, et al. Hearing dysfunction in heterozygous Mitf(Mi-wh) /+ mice, a model for Waardenburg syndrome type 2 and Tietz syndrome. *Pigment Cell Melanoma Res.* 2013;26(1):78-87.
27. Liu H, Li Y, Chen L, Zhang Q, Pan N, Nichols DH, et al. Organ of Corti and Stria Vascularis: Is there an Interdependence for Survival? *PLoS One.* 2016;11(12):e0168953.
28. Minowa O, Ikeda K, Sugitani Y, Oshima T, Nakai S, Katori Y, et al. Altered cochlear fibrocytes in a mouse model of DFN3 nonsyndromic deafness. *Science.* 1999;285(5432):1408-11.
29. Aaron KA, Pekrun K, Atkinson PJ, Billings SE, Abitbol JM, Lee IA, et al. Selection of viral capsids and promoters affects the efficacy of rescue of Tmprss3-deficient cochlea. *Mol Ther Methods Clin Dev.* 2023;30:413-28.
30. Ding D, Liu H, Qi W, Jiang H, Li Y, Wu X, et al. Ototoxic effects and mechanisms of loop diuretics. *J Otol.* 2016;11(4):145-56.
31. Chen J, Ingham N, Kelly J, Jadeja S, Goulding D, Pass J, et al. Spinster homolog 2 (spns2) deficiency causes early onset progressive hearing loss. *PLoS Genet.* 2014;10(10):e1004688.
32. Jin Z., Uhlen I., Wei-Jia K., and D. M-l. Cochlear homeostasis and its role in genetic deafness. *Journal of Otology.* 2009;4(1):15-22.
33. Homma K. The Pathological Mechanisms of Hearing Loss Caused by KCNQ1 and KCNQ4 Variants. *Biomedicines.* 2022;10(9).
34. Shubina-Oleinik O, Nist-Lund C, French C, Rockowitz S, Shearer AE, and Holt JR. Dual-vector gene therapy restores cochlear amplification and auditory sensitivity in a mouse model of DFNB16 hearing loss. *Sci Adv.* 2021;7(51):eabi7629.
35. Li Y, Ding D, Jiang H, Fu Y, and Salvi R. Co-administration of cisplatin and furosemide causes rapid and massive loss of cochlear hair cells in mice. *Neurotox Res.* 2011;20(4):307-19.

36. Elkin LA, Kay M, Higgins JJ, and Wobbrock JO. *The 34th Annual ACM Symposium on User Interface Software and Technology*. Virtual Event, USA; 2021.
37. Wobbrock J, Findlater L, Gergle D, and Higgins J. The Aligned Rank Transform for Nonparametric Factorial Analyses Using Only ANOVA Procedures. *Proceedings of the ACM Conference on Human Factors in Computing Systems (CHI '11).* 2011:143-6.

FIGURES

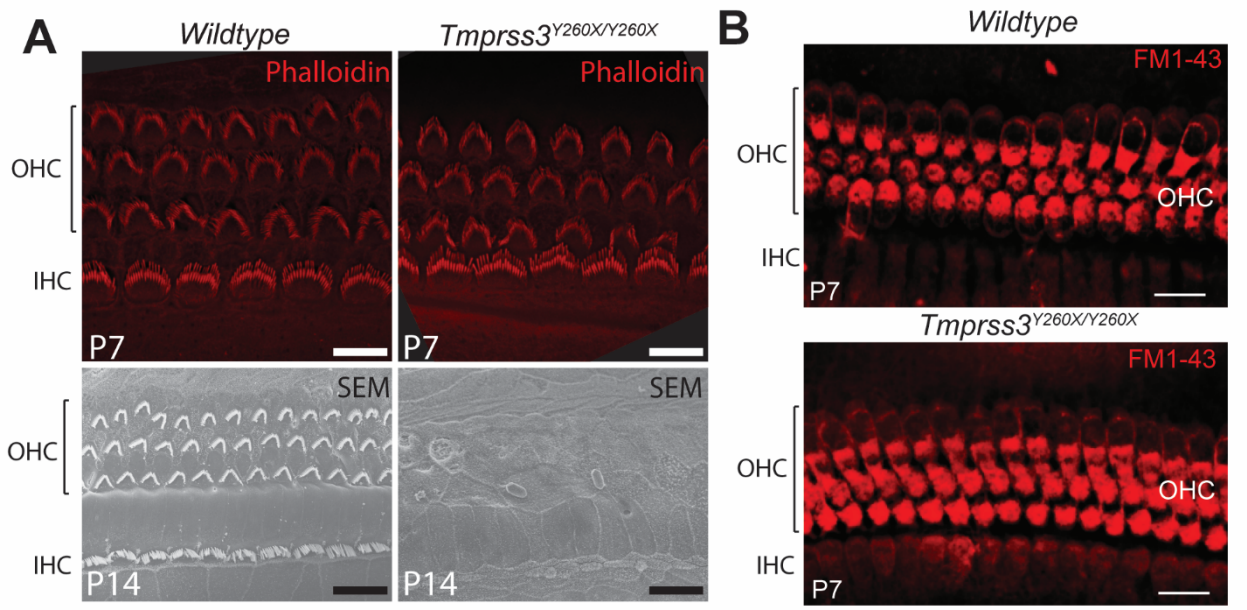

Figure 1. *Tmprss3*$^{Y260X/Y260X}$ mice demonstrate normal hair cell and stereocilia morphology and physiology prior to rapid onset degeneration.

(A) Phalloidin immunostaining and SEM microscopy shows normal architecture of inner and outer hair cells at P6 and P14 in wild-type mice, and complete hair cell degeneration at P14 in *Tmprss3*$^{Y260X/Y260X}$ mice. IHC, Inner Hair Cells, OHC, Outer Hair Cells. Scale bars, 10 μm (P7), 20 μm (P14)

(B) FM1-43 uptake by hair cells in *Tmprss3*$^{Y260X/Y260X}$ mice is equivalent compared to wild-type mice at P7. Scale bars, 20 μm

Figure 2. Spiral ganglion subtype composition is normal in *Tmprss3*$^{Y260X/Y260X}$ mice, aside from Type II SGN increase.

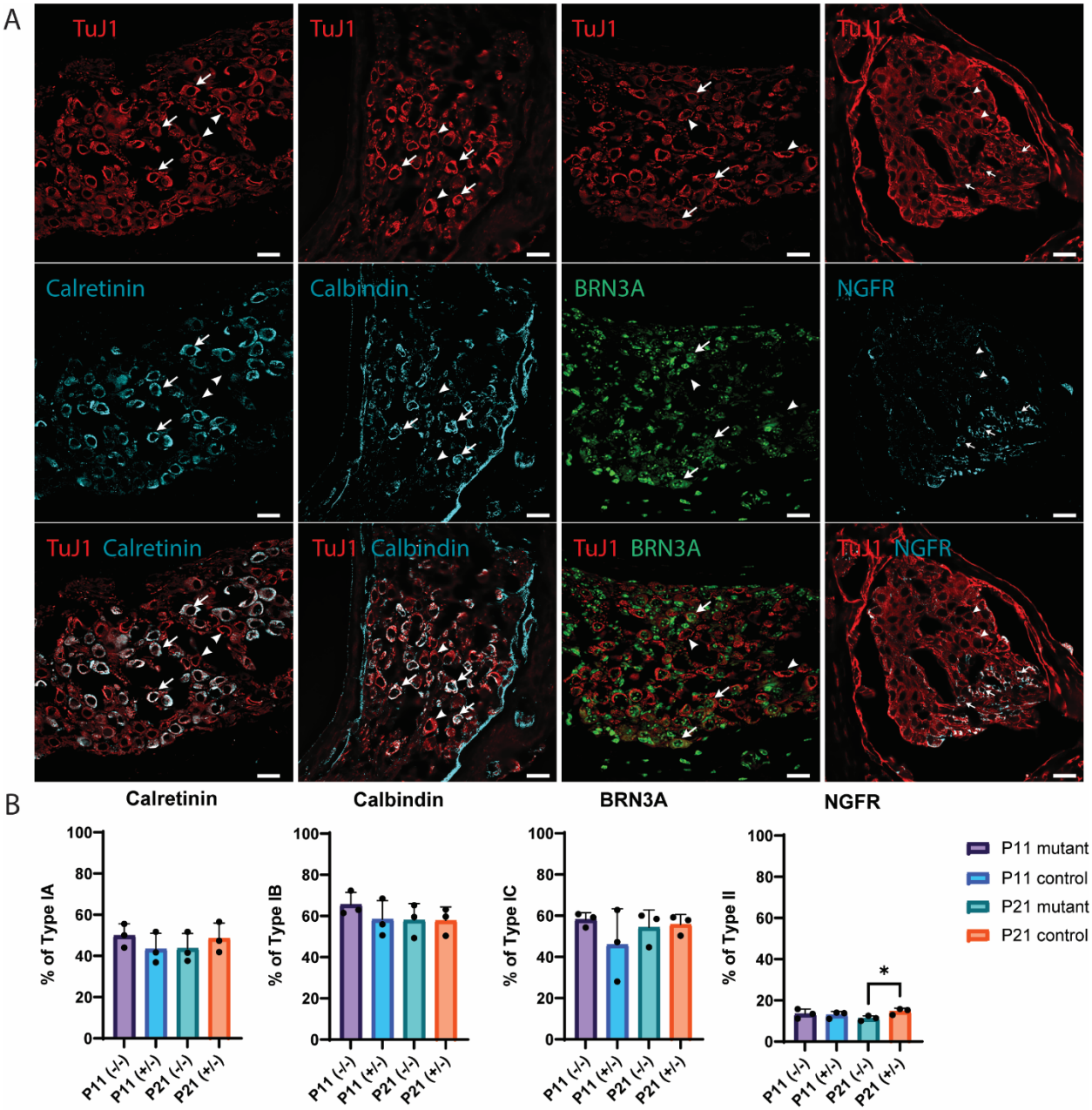

(A) Representative sections of spiral ganglion taken at P11 stained for neuron-specific class III beta-tubulin (TuJ1) and antibodies specific for Type IA spiral ganglion neurons (calretinin, CalB2), Type IB SGNs (calbindin, CalB1), Type IC SGNs (POU4F1, BRN3A), and Type II SGNs (NGFR). Top row shows TuJ1 channel, middle row shows SGN subtype-specific channel, and the bottom row shows merged channels. Arrows indicate co-staining while arrowheads indicate negative co-staining. Scale bars, 20 μm(B) Counted subtype-specific neurons at P11 and P21 for *Tmprss3*$^{Y260X/Y260X}$ and wild-type mice shows no difference aside from increased type II SGNs in wild-type mice at P21. Each point represents cell count from one cochlea (n = 3 cochleae per genotype and day).

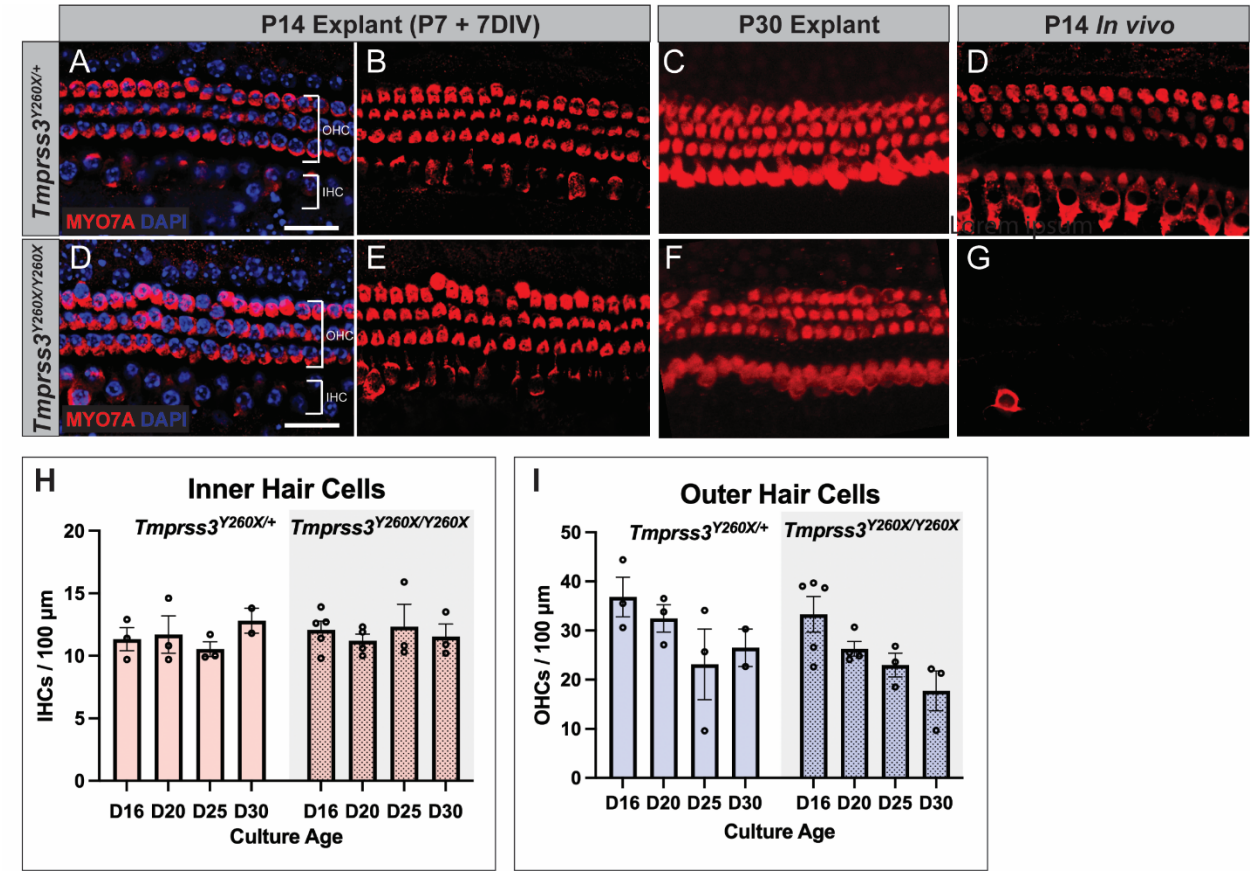

Figure 3. Cochlear explant cultures implicate intracochlear environment on hair cell death in *Tmprss3*$^{Y260X/Y260X}$ mice.

Representative images of cochlear explant cultures from control (*Tmprss3*$^{Y260X/+}$) (A, B) and *Tmprss3*$^{Y260X/Y260X}$ (D, E) mice. *Tmprss3*$^{Y260X/Y260X}$ explant at D7 with 7 days *in vitro* culture (DIV, time equivalent P14) demonstrates no hair cell degeneration of either IHCs or OHCs which is maintained to P30 explant (C, F). *Tmprss3*$^{Y260X/Y260X}$ mice display near complete hair cell degeneration at P14 *in vivo* (D, G). Scale bar, 20 µm. (H, I) Quantification of IHCs and OHCs in explant culture for control and *Tmprss3*$^{Y260X/Y260X}$ mice demonstrating slowly progressive OHC loss in both control and *Tmprss3*$^{Y260X/Y260X}$ mice. There was no significant difference in cell counts up to DIV 30 (D30) with $p > 0.11$ in all cases. Each point represents cell count from one individual culture. Exact Wilcoxon rank sum test (Mann-Whitney test) was used to compare two groups (*Tmprss3*$^{Y260X/+}$ and *Tmprss3*$^{Y260X/Y260X}$) in each culture age. Up to five cultures were quantified for each day, but only two cultures were available for D30 control (see Supporting Data Values for full details).

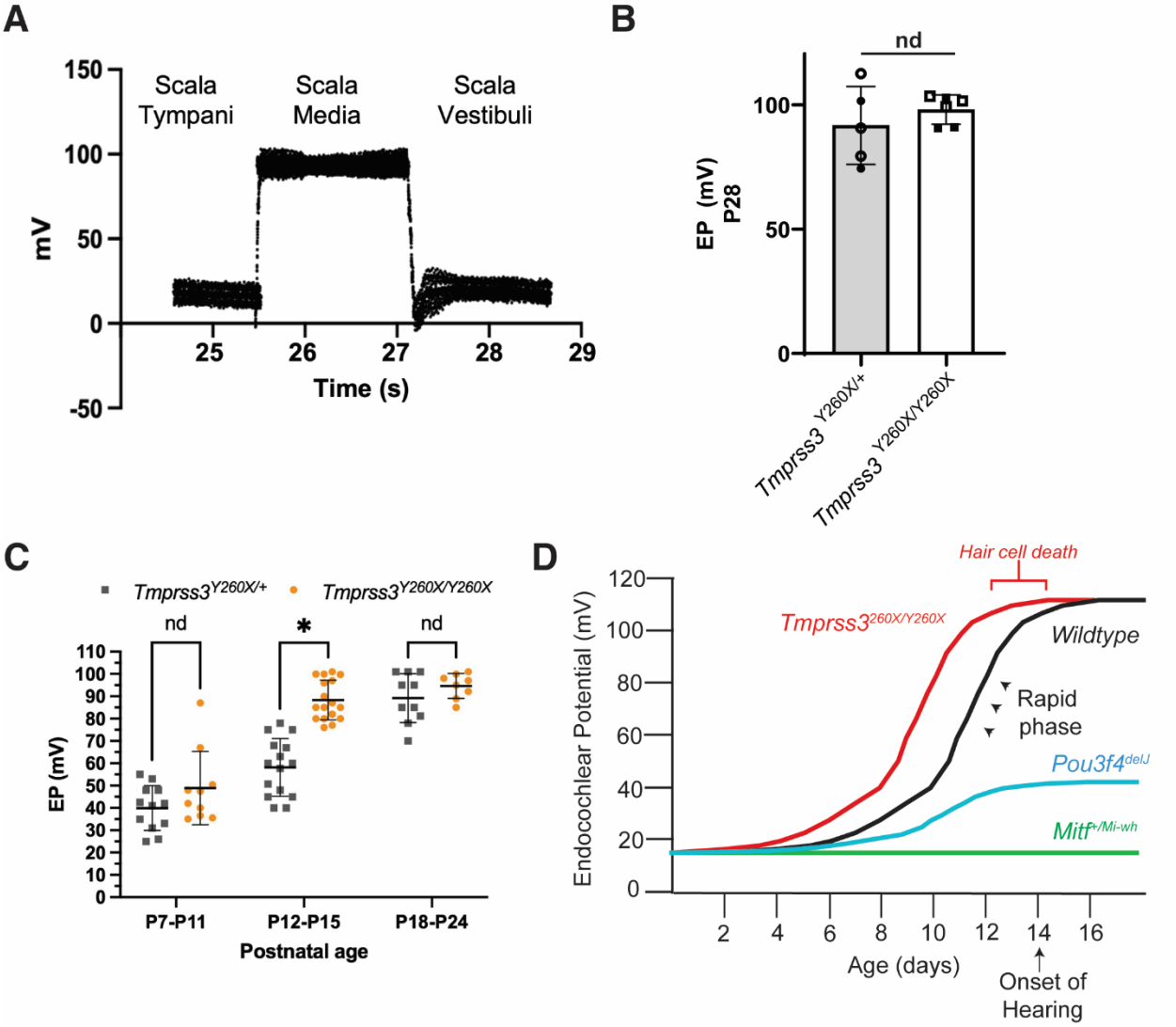

Figure 4. Direct endocochlear potential (EP) measurements show supraphysiologic rise in EP in *Tmprss3*$^{Y260X/Y260X}$ mice.

(A) EP was recorded through the basal turn of left cochleae in live mice ranging from P7-P24. Representative tracing of EP recorded from the scala media of a live control mouse.

(B) Direct EP recordings from P28 mice demonstrating no difference between control (n=5) (*Tmprss3*$^{+/-}$) and *Tmprss3*$^{Y260X/Y260X}$ (n=6) mice. Open circles and squares are females. Filled circles and squares are males.

(C) Direct EP recordings from mouse models presented here. Each data point represents one reading from one animal and plotted mean with SD. Mean EP at P12-P15 is significantly different ($p < 0.0001$) between *Tmprss3*$^{Y260X/Y260X}$ and control (*Tmprss3*$^{Y260X/+}$) mice. Wilcoxon rank sum test (Mann-Whitney test) was used to compare two groups (control, *Tmprss3*$^{Y260X/+}$ and experimental *Tmprss3*$^{Y260X/Y260X}$) in each postnatal age group (P7-11: n = 12, n = 11; P12-15: n = 15, n = 11; P18-P24: n = 10, n = 9, for control and experimental mice).

(D) Schematic demonstrating timeframe of hair cell death in *Tmprss3*$^{Y260X/Y260X}$ mice in the context of physiologic rapid phase of EP development. Both *Pou3f4*^{delJ} and *Mitf*$^{Mi\text{-}wh/+}$ knockout mice fail to generate EP and show no hair cell degeneration despite profound hearing loss.

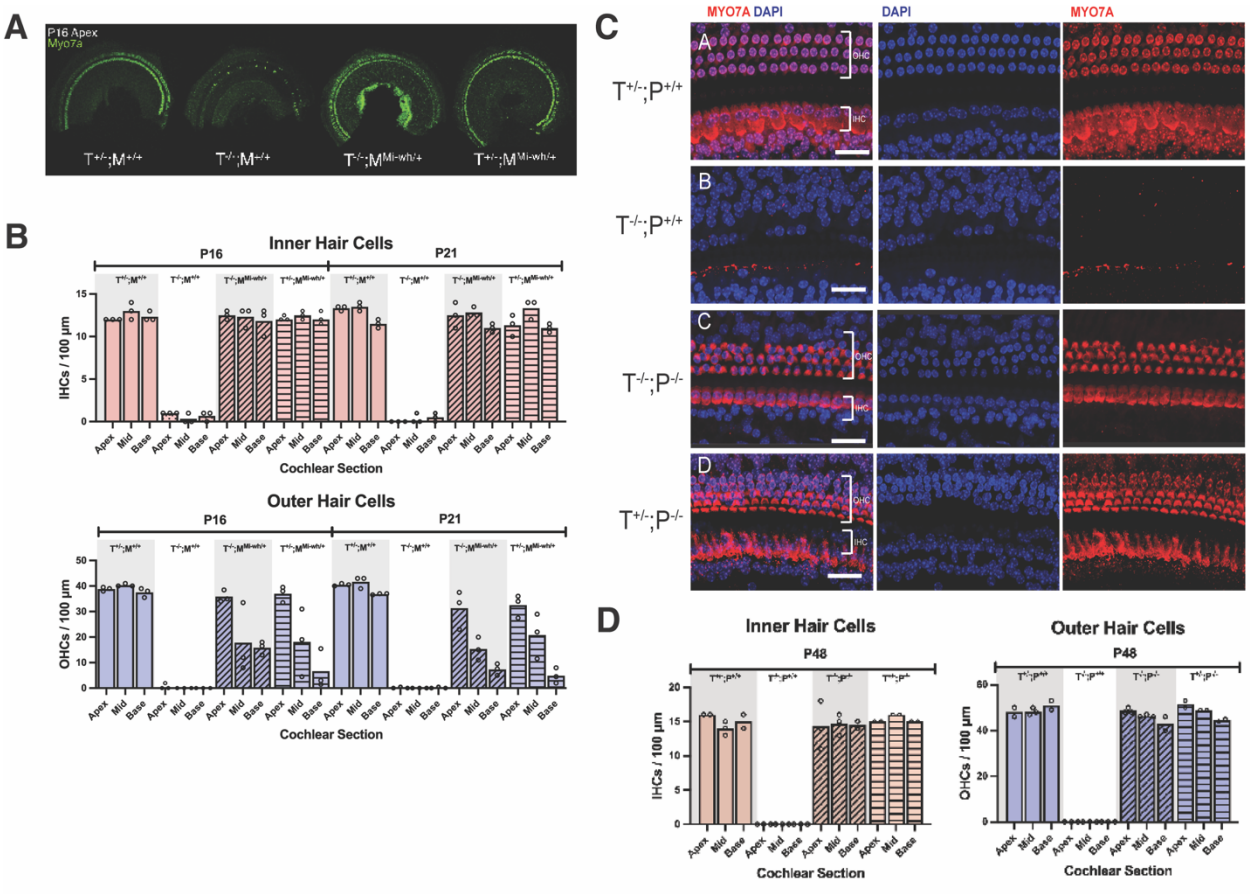

Figure 5. Rescue of cochlear hair cells in *Tmprss3*$^{Y260X/Y260X}$ mice through reduction of endocochlear potential via cross with both *Mitf*$^{Mi\text{-}wh/+}$ mice and *Pou3f4*^{delJ} mice.

(A) Representative cochlear sections of *Tmprss3*$^{Y260X/Y260X}$ ($T^{-/-}$) mice crossed *Mitf*$^{Mi\text{-}wh/+}$ ($M^{Mi\text{-}wh/+}$) mice. Sections shown are cochlear apex at P16, labelled with Myo7a.

(B) Inner hair cell and outer hair cell counts per 100 µm at P16 and P21 for $T^{-/-}$ and $M^{Mi\text{-}wh/+}$ crosses. Each dot represents the average of both ears for the same mouse. N = 3 mice per condition. Note loss of outer hair cells at P16 and P21 in $M^{Mi\text{-}wh/+}$ mouse lines.

(C) Representative cochlear sections of *Pou3f4*^{delJ} ($P^{-/-}$) crosses at P48. Cross of $P^{-/-}$ with $T^{-/-}$ mice rescues hair cells. Scale bar is 30 µM and staining is Myo7a (red) and Phalloidin (blue).

(D) Inner and outer hair cell counts for per 100 µm at P48 for *Pou3f4*^{delJ} ($P^{-/-}$) crosses. There is no loss of outer hair cells noted over time in this model. N = 2 or 3 mice per condition.

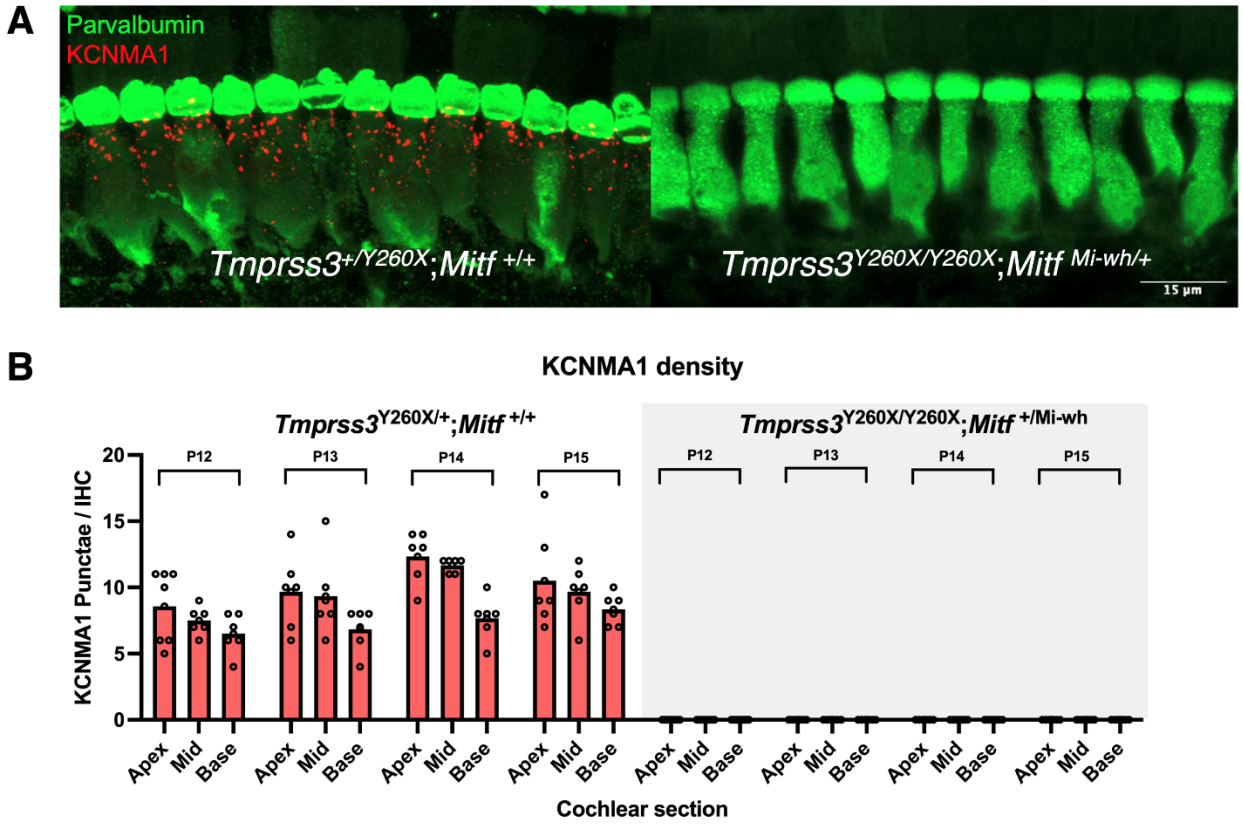

Figure 6. Reduced EP does not rescue KCNMA1 expression.

(A) Representative sections from the base of P15 cochleae from control (*Tmprss3*$^{Y260X+-}$*;Mitf*$^{+/+}$) and double mutant mice (*Tmprss3*$^{Y260X/Y260X}$*; Mitf*$^{Mi-wh/+}$) demonstrates lack of expression of the outward rectifying potassium channel KCNMA1 surviving hair cells that lack *Tmprss3* expression.

(B) Counts of KCNMA1 punctae shows base-apex gradient of expression in control mice (*Tmprss*$^{Y260X+-}$*Mitf*$^{+/+}$) at P12 (n = 9), P13 (n = 9), P14 (n = 6), P15 (n = 7) and lack of KCNMA1 expression in *Tmprss3*$^{Y260X/Y260X}$ *Mitf*$^{Mi-wh/+}$ mice at P12 (n = 9), P13 (n = 6), P14 (n = 7), and P15 (n = 6). Note that there were no punctae for *Tmprss3*$^{Y260X/Y260X}$ *Mitf*$^{Mi-wh/+}$ mice (all values were 0).

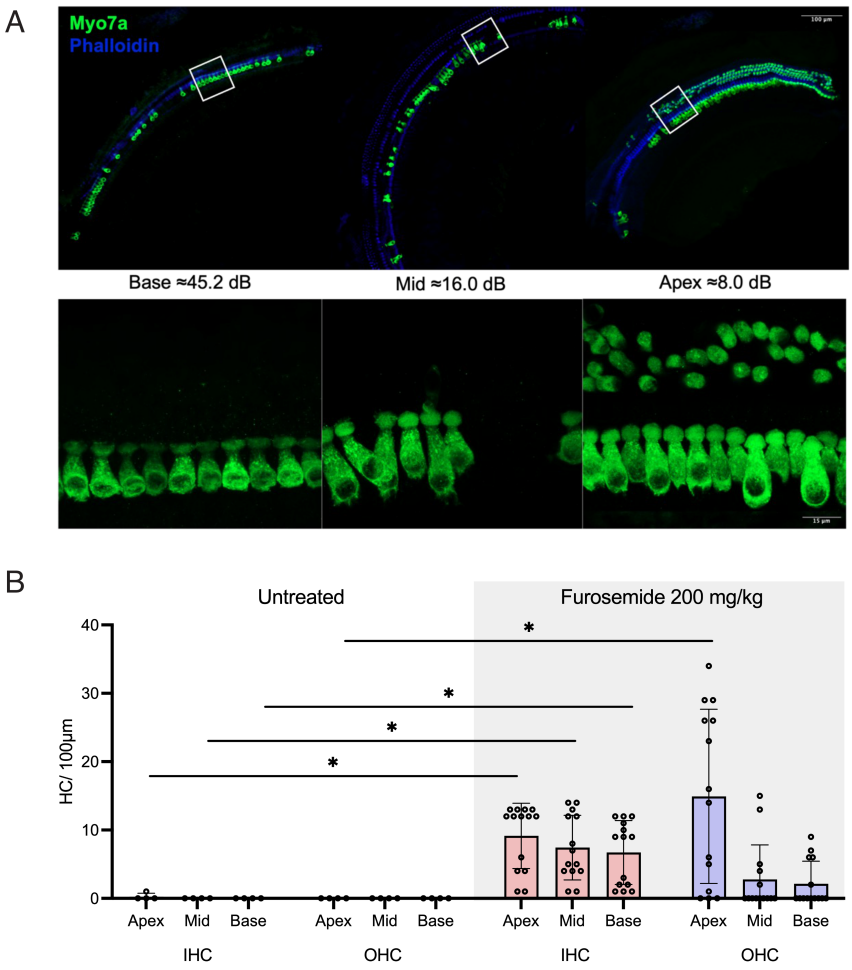

Figure 7. Pharmacologic reduction of EP using furosemide rescues hair cells.

(A) Administration of 200mg/kg Furosemide once daily from P10-P14 leads to hair cell survival in *Tmprss3*$^{Y260X/Y260X}$ mice. Representative confocal images of base, middle and apex cochlear turns of P14 *Tmprss3*$^{Y260X/Y260X}$ treated mice immunostained against Myo7a (green) and Phalloidin (blue).

(B) Mean ± SD counts of IHC and OHC counts per 100 µm sections from untreated (n=4 ears) and treated P14 *Tmprss3*$^{Y260X/Y260X}$ mice (n=7 mice) measured in the base, middle and apex cochlear turns. Each data point represents an individual cochlea. Nonparametric ANOVA with Tukey's post hoc test for comparison of untreated vs treated, IHC: p = 0.0003 for Apex, p = 0.0008 for Mid, p=0.006 for Base, and OHC: p = 0.009 for Apex, p = 0.79 for Mid, p=0.78 for Base.